SANDIA REPORT
SAND2007-7832
Unlimited Release
Printed November, 2007

New Low Cost Material Development Technique for Advancing Rapid Prototyping Manufacturing Technology

John E. Smugeresky, David D. Gill, Clinton J. Atwood

Prepared by
Sandia National Laboratories
Albuquerque, New Mexico 87185 and Livermore, California 94550

Sandia is a multiprogram laboratory operated by Sandia Corporation,
a Lockheed Martin Company, for the United States Department of Energy's
National Nuclear Security Administration under Contract DE-AC04-94AL85000.

Issued by Sandia National Laboratories, operated for the United States Department of Energy by Sandia Corporation.

Available to DOE and DOE contractors from
U.S. Department of Energy
Office of Scientific and Technical Information
P.O. Box 62
Oak Ridge, TN 37831

Telephone: (865) 576-8401
Facsimile: (865) 576-5728
E-Mail: reports@adonis.osti.gov
Online ordering: http://www.osti.gov/bridge

Available to the public from
U.S. Department of Commerce
National Technical Information Service
5285 Port Royal Rd.
Springfield, VA 22161

Telephone: (800) 553-6847
Facsimile: (703) 605-6900
E-Mail: orders@ntis.fedworld.gov
Online order: http://www.ntis.gov/help/ordermethods.asp?loc=7-4-0#online

SAND2007-7832
Unlimited Release
Printed November, 2007

New Low Cost Material Development Technique for Advancing Rapid Prototyping Manufacturing Technology

John E. Smugeresky
Analytical Materials Science Department
Sandia National Laboratories
P.O. Box 969
Livermore, CA 94550

David D. Gill and Clinton J. Atwood
MesoScale Manufacturing and Systems Development Department
Sandia National Laboratories
P.O. Box 5800
Albuquerque, New Mexico 87185-MS1245

Abstract

The world's rapidly evolving threat environment has shown the need for a responsive infrastructure that can address changing requirements with agility and confidence. While this need has often been associated with the design and fabrication of new components, it is noteworthy that there will be instances in which new materials and alloys will be required to meet the demands of new component designs. Past efforts to perform rapid alloying studies have shown some success, but metallurgical properties were adversely affected by changed cooling profiles during production scale-up. The purpose of this research was to perform rapid alloying studies using the Laser Engineered Net Shaping™(LENS®) rapid manufacturing process. The process can be used for both alloying studies and for the creation of the final components in the same materials and at the same size scale, so prototype attributes would also be present in the final components.

Alloying studies included stainless steel enhancements with iron and manganese, as well as iron-manganese and iron-nickel alloy systems. The alloying studies demonstrated the creation of unique microstructures and a feasible method of creating many alloy compositions in small samples limiting both cost and waste. Unfortunately, ongoing porosity problems reduced the impact of the study. Process parameters affecting porosity were identified, but starting powder characteristics impacted the overall porosity to a larger extent than was expected.

ACKNOWLEDGMENTS

The authors wish to acknowledge Andy Gardea for metallographic sample preparation, microhardness measurements, and optical microscopy, Jeff Chames for SEM and EDS analyses, and Miles Clift, for EDX analyses and compositional mapping.

TABLE OF CONTENTS

1. Introduction 9

2. Experimental Approach: Past and Present 11
   - 2.1 Past Research Efforts 11
   - 2.2 The Planned Technical Approach 11
   - 2.3 The Planned Approach to the Analysis of Graded Samples 12
   - 2.4 Key R&D Goals and Project Milestones 12

3. Outline of the Experiments 13
   - 3.1. Materials 13
   - 3.2. Sample Fabrication 13
     - 3.2.1. LENS Process Variables 13
     - 3.2.2. LENS Deposition of FeMn 14
     - 3.2.3. LENS Deposition of FeNi 16
     - 3.2.4. Environment, Safety, and Health Considerations for Depositing Nickel Powder with LENS 17
     - 3.2.5. LENS Produced Sample Sets and Process Settings 17
   - 3.3. Sample Analysis 18

4. Results 21
   - 4.1. SET 1: Reference Matrices: Atomized 316 SS, Sponge Iron 21
   - 4.2. SET 2 (A) Baseline 316L SS “Alloys”: Fe vs. Mn 22
   - 4.3. SET 3 (B) Fe-10%Mn; Fe-14%Mn Alloys: Atomized Iron: 24
   - 4.4. SET 4 (D) Atomized Iron Only; Closed Loop Control: 24
   - 4.5. SET 5 (E) Four Fe-Mn Alloy Tensile Bars: Closed Loop Control 26
   - 4.6. SET 6 (F) Four Fe-Mn Alloy Tensile Bars, Closed Loop Control; Duplicates 27
   - 4.7. SET 7 (G) Fe-20Mn, Fe-10Mn: Effect of Threshold Setting 28
   - 4.8. SET 8 (H) Fe-5, 10, 20% Ni: Filter Density Effect: 200 vs. 180% 28
   - 4.9. SET 9 (J) Fe-20% Ni: Effect of Laser Power; 355, 480, 650, 955W 30
   - 4.10. SET 10 (K) Fe-20% Mn: Effect of Laser Power; 245, 355, 480, 650W 31

5. Discussion 33
   - 5.1. Reference Experiments 33
   - 5.2. Iron-Manganese and Iron-Nickel Systems 33
   - 5.3. Appropriateness of the Technique 34

6. Conclusions 35

7. References 36

LIST OF FIGURES

Figure 1: Melt Pool Images of Iron at 915W (left) and Stainless 316L at 500W (right) Showing a Comparison of the Relative Sizes of the Melt Pool. 15
Figure 2. Melt Pool Images of 80-20 FeMn Alloy at Various Power Levels. 16
Figure 3. Melt Pool Images of 80-20 FeNi Alloy at Various Power Levels. 17
Figure 4. Cross-Sections of Three Samples with 316L Only (top), and Fe Added at Two Values in Open Loop (left) and Closed Loop (right) Control Modes. 21
Figure 5. The As-Polished Samples Indicate that the Uniformity in Cross Section is Better in Open Loop than Closed Loop Control, but Porosity Is Still above Acceptable Levels in Both. 22
Figure 6. Composition Profiles for Iron Added to 316L SS (left), and Manganese Added to 316L SS (right). 23
Figure 7. Hardness Profiles for Iron (SF1A) and Manganese (SM2a) Added to 316L SS. 23
Figure 8. Composition Map Showing Overlay of BSE Image and Mn Distribution (light green hue), Indicating Incomplete Melting of the Stainless Steel Particles. 24
Figure 9. As-Polished Cross Section of Sample F1-B, Showing Porosity and Poor Inter-Layer Bonding. 25
Figure 10. Polished Cross Sections of the Pure Iron Cubes (F2D, F3D) and the Horizontal Tensile Bar (F4D-1, F4D-2), Showing 1% Porosity 25
Figure 11. Schematic Cross Sections of FeMn Showing Target Compositions Under Closed Loop Control. 26
Figure 12. Cross Section of FeMn Sample FM1E with Location and Measured Composition Mapped on Surface. 26
Figure 13. As-Polished and Schematic Cross Sections of the FeMn Sample FM25-1F(left) and FMX-2F (right) Showing Target Compositions, Interface Regions, and Porosity. 27
Figure 14. Plot of Hardness vs. Mn Content Indicating an Initial Increase with 10 % Mn Levelling to 75% Mn. 27
Figure 15. Schematic Cross Section of Fe-10% Mn and Fe-20% Mn Samples and Polished Cross Section of Fe-10% Mn Showing Porosity, Layer Interfaces (Dotted Lines) and Threshold Setting Changes. 28
Figure 16. Plot of Laser Power (Watts) vs. Threshold Settings for Fe-10% Mn and Fe-20% Mn Showing that Increased Mn Content Reduces the Power Required to Maintain a Specific Melt Pool Size 29
Figure 17. Cross Section of Sample FN1H for Filter Setting of 200% and Threshold Intensity of 200, Showing Variation of Porosity with Composition. 29
Figure 18. Cross Section of Sample FN-2H for Filter Setting of 180% and Threshold Intensity of 200, Showing Variation of Porosity with Composition. 30
Figure 19. Hardness Profile with Location and Nominal Compositions for the FeNi Binary System. 30
Figure 20. Cross Section of Fe-20%Ni Samples Deposited with Laser Power of 355W (left) and 955W (right) Showing an Increase in Pore Size and Inter-Layer Bonding with Increased Power. 31
Figure 21. Cross Section of Fe-20%Mn Samples Deposited with Laser Power of 245W (left) and 650W (right) Showing an Increase in Pore Size and Inter-Layer Bonding with Increased Power. 31

LIST OF TABLES

Table 1. Project Goals and Milestones. 12
Table 2. LENS Process Variables. 14
Table 3. Powder Feeder Speeds for Various Material Compositions. 15

1. INTRODUCTION

The purpose of this work was to address Sandia's mission for a responsive manufacturing infrastructure by providing a means to explore, fabricate, and evaluate new alloy compositions to meet emerging threats in a timely manner. The project team explored the use of the LENS® process, an additive rapid prototyping manufacturing technology, to create advanced, novel, and non-traditional materials using laser beams and powdered metal particles. This technology examines the degree to which composition and microstructures can be engineered during manufacturing of parts to near net-shape. The project focused on iron-based alloys of interest for Sandia's traditional structural components. The project team identified the potential for LENS to provide a tool for expanding the available materials over a range of size scales, from the conventional micrometer range to the nanocrystalline regime. In any event, LENS will be a value to all Sandia SMU's as a tool for accelerating the transition from engineering concept to prototype to production of new designs.

The scope of this work consisted of fabricating and evaluating several series of iron-based alloys with iron, nickel, manganese, and austenitic stainless steel to demonstrate the alloy development capability using the LENS® Process. Two sizes of small coupons of varying composition were made to either evaluate the microstructure, hardness, and composition or to measure mechanical properties in tension. It was also intended to document the process parameter space for making sound metallurgical specimens.

2. EXPERIMENTAL APPROACH: PAST AND PRESENT

Past alloying research has identified unique alloy characteristics that rely on rapid solidification of the material. These advantages have been lost at production scale-up, and this experience has influenced the planned experimental approach for this project.

2.1 Past Research Efforts

Previous efforts in rapid solidification alloying have shown the opportunity to achieve enhanced microstructure, but the techniques have not been utilized due to their inability to be scaled. When scaled, rapid solidification was lost as were the unique microstructures originally achieved in prototype alloy testing. LENS offers the opportunity to achieve rapid solidification in the alloy development process, as well as in the part creation process because both will be done on the same machine and in the same relative size of geometry.

Current methods of material development for WR and other components consume large quantities of material, money, and time while producing excessive waste in the form of non-performing alloys. The proposed research will revolutionize the alloy development process so that it is capable of addressing emerging threats in a timely manner and reduced budget while also reducing waste. To meet the challenges of emerging threats, including the loss of manufacturing capabilities to offshore venues, we must have alternate ways to more quickly bring new materials and products from concept to deployment. Laser additive manufacturing has matured as a technology that can not only make prototype parts quickly, but can also do the actual production of small lot sizes, typical of our defense systems, and if need be, repair or upgrade expensive parts quickly and cheaply. The idea proposed here is to use this non-conventional technique (laser based additive manufacturing), as a new material synthesis methodology to explore new or modified alloy compositions over composition ranges far greater than possible with conventional processes. The team hoped to demonstrate the ability to do this more quickly and inexpensively than is currently possible by utilizing graded composition samples synthesized by adding and mixing different constituents under precise computer control to vary composition on a millimeter scale basis while still allowing a complete spectrum of alloy compositions. The resulting scaled samples will be ideally suited for sophisticated materials analysis including SEM, EDS, and EDX for phase identity, volume fractions, and phase boundaries resulting in a complete phase diagram (characterization) study. Only the compositions with the most promising microstructures and associated properties will need to be evaluated during scale up.

2.2 The Planned Technical Approach

The initial demonstration was done using a model binary system with selected elements of alloys used for defense applications. We expected to use at least one candidate from: multi-element self-sharpening bulk glass forming alloys, ultra-fine grain high strength high impact resistant ductile steels for penetrator case applications, titanium alloys for biomedical applications, inexpensive corrosion resistant alloys for weapon cases, metal matrix blast resistant composites for response to emerging terrorist threats, and a simple but deep Fe-based eutectic to probe the effects of adding third and fourth elements on the compositional location and melting point of the eutectic. This would enable development of multi-element bulk glass forming alloys, and/or precursors for ultra-fine grain materials. A fundamental principle suggests adding metalloids that will deepen the eutectic, and enhance the likelihood of glass phase formation, especially

under the high cooling rates of laser assisted additive manufacturing. Even if the cooling/solidification rates realized are not high enough to achieve a glassy phase, the metalloids will act as both nucleation sites and assist in pinning grain boundaries so an ultra-fine or even nanocrystalline size grain microstructure might be created. Synthesis will include at least one titanium rich alloy, adding elements to stabilize the beta phase and adding a third and possible fourth element to refine the grain size or inhibit columnar growth. A final candidate material system is tantalum alloys that can be used for aerospace rocket nozzle applications to increase erosion resistance.

2.3 The Planned Approach to the Analysis of Graded Samples

The analysis of the graded samples was limited to metallographic sample preparation for optical microstructure analysis, micro-hardness, and SEM evaluation using EDS for phase identification and characterization. Mechanical properties were done on select compositions after initial microstructure and phase analysis (dependent on application for specific alloy systems). Composition-dependent process modeling to assess how composition gradients affect the molten pool area control system was planned but not completed. Because it is an advanced manufacturing system, the additive manufacturing uses a closed-loop feedback system that is dependent on the emissivity of the molten pool to control the melting conditions. Because previous additive manufacturing materials have been of constant composition, emissivity had been presumed constant as well. However, in graded materials, emissivity varies with composition, and some modeling was expected to be required to estimate these effects before making the materials. For example, an exothermic heat of mixing can enhance melting and alloying while reducing the required laser power. The opposite is true for an endothermic reaction, where we may be power limited for maintaining the molten pool as powder is added. In addition, crossing a phase boundary would also impact the emissivity. To model these effects, we will apply thermodynamic process modeling to generate predicted phase diagrams, relevant enthalpies, and melt pool parameters. Using these results, we can provide compositionally adaptive process control, guarantee accurate powder feeding, monitor powder flow by constituent, and assure substrate compatibility.

2.4 Key R&D Goals and Project Milestones

The project was a 2 year LDRD project and the project proposal contained the following R&D goals and milestones.

Table 1. Project Goals and Milestones.

Goal/Milestone	Completion
Tests Completed Showing Weld Pool Control Needed to Adapt to Changing Composition	Q1, FY06
Computer Modeling Predicts 2 Alloy Compositions Ranges of Interest	Q2, FY06
Material Samples Completed for 2 Alloying Sample Matrices	Q3, FY06
Microstructure and Microhardness Evaluation of 2 Sample Sets Completed	Q4, FY06
One or More Compositions Selected for Repeatability Analysis and Scale-Up for Production	Q1, FY07
Modeling Completed for 3 Additional Compositions	Q2, FY07
Material Samples Completed for 3 Additional and 1 Repeatability Compositions	Q3, FY07
Material Analysis, Final Reports, and Journal Manuscripts Completed	Q4, FY07

3. OUTLINE OF THE EXPERIMENTS

3.1. Materials

Elemental and pre-alloyed powders were purchased from various suppliers. Not all powders of interest were available as gas atomized. Manganese was more difficult to get than nickel, iron, or 316 stainless steel. The powder size of interest was 45 to 105 microns (-100 + 325 mesh). While gas atomized nickel powder was available, iron and manganese were not. The team tried two types of iron from Hoeganaes Corporation: chemically precipitated sponge (ANCOR MH-100), and water atomized (Ancorsteel 1000B). The Ancorsteel 1000B powder produced better samples. The 316 SS was gas-atomized powder, -100 +325 mesh (150 to 44 microns) obtained from Carpenter Corporation. Manganese was Cerac M-1133, -140 +325 mesh (100 to 44 microns), 99.6 % pure, very expensive ($155.00/lb, 22 lbs.) and master iron-manganese alloys (Ferro-manganese) were also explored for evaluation for Mn alloying due to lack of availability of more pure or atomized manganese. Generally, the powders needed to be resized or ordered to a specification quite different from what is the typical size range for the other processes, which resulted in delays for delivery of 4-5 weeks. The nickel from Crucible was 99.5% pure, Heat# 521-274, particle size -100+270 mesh (150 to 53 microns) size fraction.

The substrates were made out of 304L SS. Nominal sample size was 9.5 by 9.5 by 9.5 mm (3/8 by 3/8 by 3/8 inches) for metallographic and compositional analysis. For tensile mechanical property evaluations, sample sizes of 3/8 by 2 by 3/8 inches (9.5 by 51 by 9.5 mm) were fabricated.

3.2. Sample Fabrication

An Optomec LENS® system powered with a 1 KW Nd:YAG laser was equipped with two powder feeders and a closed loop feedback control system. The feedback system is based on high speed imaging of the molten pool to maintain constant solidification conditions by controlling melt pool size. Experiments were done with and without melt pool feedback control. Powder flow rate was determined for a range of auger rpm by flowing powder into a collection bag and weighing the bags after a known interval of time. Changing the relative rotation speed of the two feeders, prescribed alloy compositions were prepared. Samples were also made in open loop mode due to differences in emissivity associated with alloying element additions. The differences in emissivity cause over exposure to the camera sensors, making them ineffective in controlling some alloy combinations. Samples were prepared in an argon atmosphere with oxygen kept below 5ppm.

3.2.1. LENS Process Variables

There are many process variables associated with LENS deposition that have a direct effect on the overall quality of the part produced. An indication of part quality in the LENS process is the amount of porosity present in the material. While there is an attempt to control the most important process variable, laser power, using a closed loop system, there is still a heavy reliance on operator intuition to determine the appropriate settings for each individual build. This knowledge is generally gained through years of experience and previously recorded parameter logs and build data. While most of the process variables remain fairly constant regardless of

material, others may change significantly throughout the development. The LENS process variables are shown below in Table 2.

Table 2. LENS Process Variables.

-Global Variables-	-Closed Loop Variables-	-Open Loop Variables-
Powder Flow Rate*	Neutral Density Camera Filter*	Laser Power*
Layer Thickness*	Threshold Intensity*	
Hatch Width*	Border Pixel Area*	
Hatch Angle Increment*	Fill Pixel Area*	
Embed Depth	Overhang Pixel Area	
Deposition Speed	Proportional Gain	
	Integral Time	
	Derivative Time	
	Shutter Count Delay	
	Offset Volts	

*Significant Process Variable for FeMn / FeNi Deposition

3.2.2. LENS Deposition of FeMn

The process development for FeMn first began with an attempt to deposit pure iron on a stainless steel substrate. Since iron is the majority balance of the alloy composition it is important to develop these parameters first and then to begin adding the manganese element and adjust parameters accordingly. A brief literature search revealed very little information with regard to previous experience with iron in the LENS process and no information regarding manganese deposition. To help in the initial development, the closed loop control system was disabled and the laser power was manually set and adjusted. This helps build a strong baseline indication of the approximate power level needed to achieve successful deposition. Initially, iron looked to deposit best when the laser power was in the upper band, averaging around 915 watts. While this power level was rather high compared to a typical steel deposition, the drawn lines were forming nicely and the overall height and shape of the part looked sufficient. Figure 1 shows an image of the iron melt pool during the initial development compared to the typical melt pool seen during 316L stainless steel deposition.

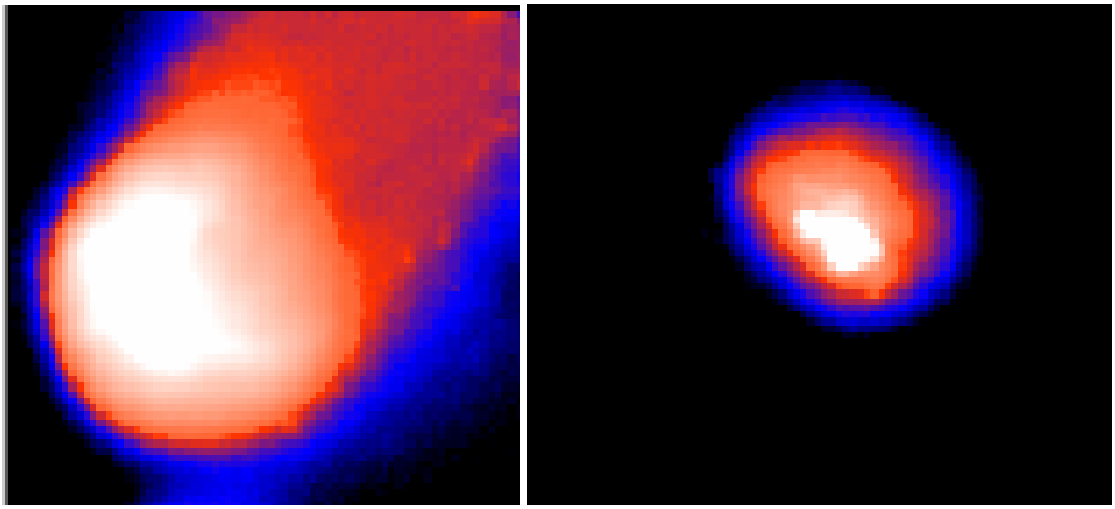

Figure 1: Melt Pool Images of Iron at 915W (left) and Stainless 316L at 500W (right) Showing a Comparison of the Relative Sizes of the Melt Pool.

As shown in Figure 1, the initial iron melt pool is extremely large and has an intense heat signature, formed as a direct result of the 900 watt laser power. The drastic contrast between the two images was troubling and the resultant metallographic sample showed large voids in the part. An adjustment was made to several global process variables to help reduce laser power in hopes of reducing the part porosity, all while maintaining adequate shape and height. In particular, the slice thickness was reduced from 0.020" to 0.010" (0.51 to 0.25mm) and the hatch width was reduced from 0.020" to 0.015" (0.51 to 0.38mm). Subsequent tests confirmed less porosity with less power. An average power setting of 500 watts was established after further development, and confirmed with metallographic analysis. Once a power band has been established manually, the closed loop control system was enabled and adjusted to reflect this power level.

Once the process parameters for iron were firmly established, manganese was gradually added, initially only 5%, to the powder stream using a second feeder. The powder flow rate for each material is adjusted to always maintain a constant flow into the melt pool at 26.5 grams per minute. Table 3 shows the various powder feeder speeds for different alloy compositions.

Table 3. Powder Feeder Speeds for Various Material Compositions.

Composition	gram/min Fe	gram/min Mn	RPM Fe	RPM Mn
100% Fe	26.5	0	525	0
95%Fe, 5%Mn	25	1.325	500	66.5
90%Fe, 10%Mn	23.85	2.65	477	93
80%Fe, 20%Mn	21.2	5.3	424	146
75%Fe, 25%Mn	19.88	6.62	398	172
50%Fe, 50%Mn	13.3	13.2	266	304
25%Fe, 75%Mn	6.7	19.8	134	436
100%Mn	0	26.5	0	570

The addition of manganese powder greatly affected the melt pool with a sharp increase in image intensity due to difference in the emissivity of manganese. The closed loop controller

immediately detected increase in intensity and reduced the laser power accordingly. The system initially maintained approximately 285 watts of power with the addition of manganese. The closed loop system variables were then adjusted to maintain power in the range that iron showed the least amount of porosity, approx. 500 watts. The resulting metallographic analysis showed large amounts of porosity in the FeMn alloy. A test matrix was developed to best determine the correct power level to minimize part porosity in the FeMn alloy. A fixed material composition of Fe – 20%Mn was selected for the study. The closed loop control system was disabled and the power levels were manually set in increments of approximately 100W. A total of four different cubes were built, each with a different laser power level. Melt pool images of each test are shown below.

Figure 2 highlights the effect of adding manganese to the melt pool. A much brighter reflection is present in the images and, thus, explains the drop in laser power. A complete metallographic analysis of each sample was performed to quantify the level of porosity in the material.

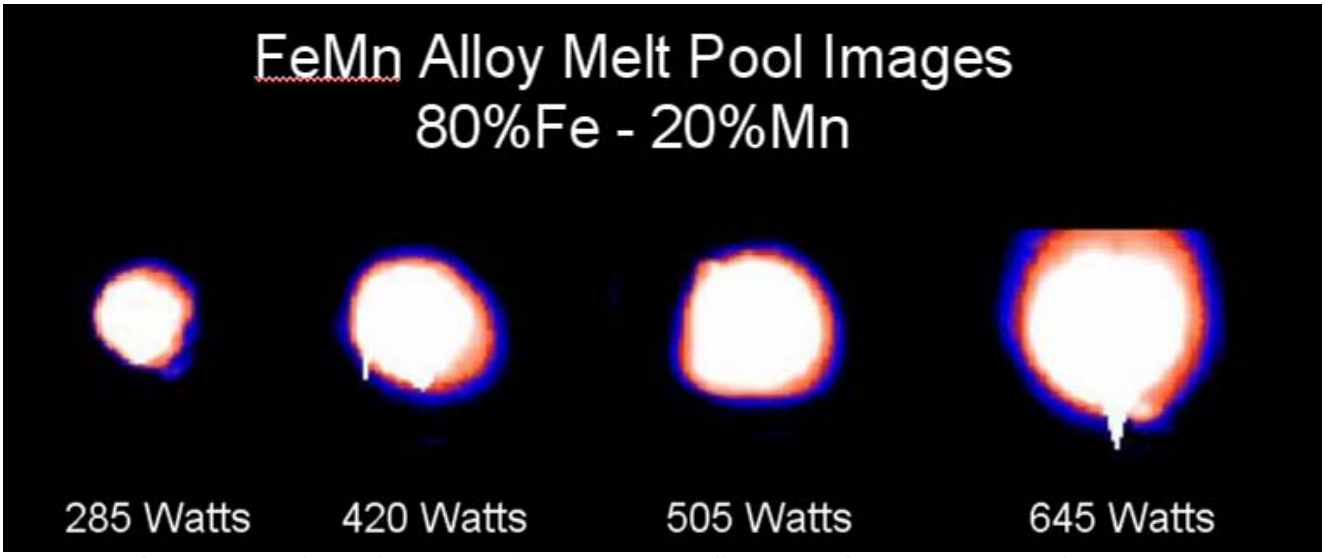

Figure 2. Melt Pool Images of 80-20 FeMn Alloy at Various Power Levels.

3.2.3. LENS Deposition of FeNi

The process development for FeNi was very similar to that of FeMn; however, the addition of nickel powder into the melt pool did not produce a brighter reflection and did not reduce the laser power. Instead, the power was maintained near the optimal power setting for iron, at 500W. A test matrix was also developed to measure porosity levels at various power settings. A fixed material composition of 80%Fe – 20%Ni was chosen for the study. The closed loop control system was disabled and the power levels were manually set three different intervals. Melt pool images of each test are shown below.

Figure 3 illustrates the effect of adding nickel powder to the iron melt pool. These images are more representative of traditional melt pools for stainless steel and iron. A complete metallographic analysis of each sample was performed.

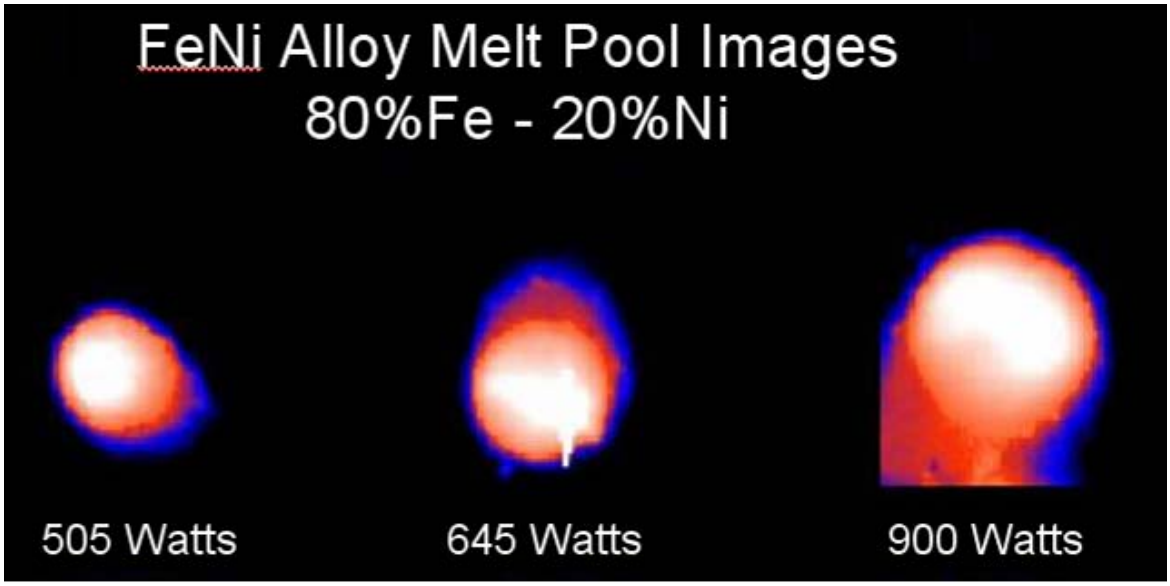

Figure 3. Melt Pool Images of 80-20 FeNi Alloy at Various Power Levels.

3.2.4. Environment, Safety, and Health Considerations for Depositing Nickel Powder with LENS

The handling and processing of nickel powder in the LENS laboratory required special considerations and documented procedures, as nickel powder is considered a particularly hazardous substance by laboratory standards. A thorough review of ES&H guidelines and direct consultation with an industrial hygiene representative resulted in a formal operating procedure for all nickel powder interaction within the laboratory. The most important area of concern is during the cleaning of the LENS system glove box. This activity places operators in direct contact with nickel powder. The operating procedure for the box cleanout provides guidelines on use of personal protective equipment (PPE), including the use of a full face respirator with HEPA filters, full length Tyvek coveralls with booties and double disposable gloves taped to the Tyvek suit. 6-mil plastic is used to contain powder around the work area and a HEPA vacuum is used to control the dust. The document developed will serves as a template for future hazardous material processing in the LENS laboratory.

3.2.5. LENS Produced Sample Sets and Process Settings

Nominal or baseline deposition conditions for 316L SS were laser power of 810 watts (36 amps current), 0.020 inch (0.51 mm) layers, 0.020 inch (0.51 mm) line trace spacing, 20 ipm (8.5 mm/s) travel speed and about 31.3 grams per minute powder feed rate, with or without the use of a feedback sensor control system to control the solidification conditions with a fixed size for the molten pool. Under closed loop control, the laser power varies from 360 to 965 watts power (25 to 40 amps) with geometry and distance from the substrate to maintain a fixed molten pool size. Without such control, the molten pool size varies with position from the substrate and is somewhat path dependent, but certainly dependent on whether a thin or thick region of sample shape was being formed,

Thirty three samples were fabricated in ten sets of experiments, each evaluating a specific effect.
SET 1 Reference Matrices: Atomized 316 SS, Sponge Iron (6 samples)

- Gas Atomized 316 SS, ANCOR MH-100 Sponge Iron, and 316 SS with Iron Added
- (S1, S2, F3, F4, SF5, SF6)
- (5/17/06)

SET 2 (A) Baseline 316L SS "Alloys": Fe vs. Mn (2 samples)

- (Sample IDs are: SF1A, and SM2A (06M144, 06M145)
- (5/22/06)

SET 3 (B) Fe-10%Mn; Fe-14%Mn Alloys: Atomized Iron (4 samples)

- Ancorsteel 1000B, Water Atomized Iron
- (Sample IDs are: FI-B, F2-B, FM-3B, and FM4-14)
- (EO06-143) 6/8/06

SET 4 (D) Atomized Iron Only; Closed Loop Control (4 samples)

- Atomized Ancorsteel 1000B Iron
- EO07-064 (1-16-07)
- (Sample IDs are: F1D, F2D, F3D, and F4D)

SET 5 (E) Four Fe-Mn Alloy Tensile Bars: Closed Loop Control (3 samples)

- 0, 5, 10, and 20 Wt. % Mn; Sample IDs are: FM1E and FM2E
- 0, 25, 50, and 75 Wt. % Mn; Sample ID is: FM3E)

SET 6 (F) Four Fe-Mn Alloy Tensile Bars, Duplicates (2 samples)

- (Sample IDs are: FM25-1F, FMX-2F

SET 7 (G) Fe-20Mn, Fe-10Mn: Effect of Threshold Setting (2 samples)

- Fe-xMn: Characterize And Reduce Porosity
- "Effect of Threshold on Power as f(Position, Composition)"
- (Sample IDs are: FM20-2G; FM10-3G

SET 8 (H) Fe-5, 10, 20% Ni: Filter Density Effect: 200 vs. 180% (2 samples)

- "Effect of Filter Density on Laser Power"
- EO07-128 (5-10-07)
    - Sample IDs: FN1H (200%), and FN2H (180%)

SET 9 (J) Fe-20% Ni: Effect of Laser Power; 355, 480, 650, 955W (4 samples)

- EO07-128 (5-10-07)
- Sample IDs: FN20-W-XJ, (W-X= 355-5, 480-3, 650-6, 955-4 (Watts-No.))

SET 10 (K) Fe-20% Mn: Effect of Laser Power; 245, 355, 480, 650 W (4 samples)

- EO07-129 (5-10-07)
- Sample IDs: FM20-W-XK, (W-X= 245-4, 355-1, 480-2, or 650-3 (Watts-No.))

3.3. Sample Analysis

Samples were sectioned perpendicular to the deposition planes and perpendicular to the top layer deposition direction. This allowed observation of layer thickness, deposition path overlap, and differences between effective layer thickness (determined by interlayer vertical height increments) and actual layer thickness (determined by processing parameters and only observable at the topmost layer cross-section). Standard metallographic grinding and polishing procedures were used to prepare as-polished surfaces for porosity evaluation, SEM backscattered imaging, and compositional determination and mapping with EDS and electron microprobe

wavelength analyses. Samples were observed in the as-polished condition to look for porosity, determine composition and for composition mapping in both the SEM and the microprobe. Where necessary, carbon coating was applied for SEM observations of microstructure. Image processing software was used to determine fractional porosities. Selected samples were etched for secondary electron SEM and optical microscopic observation and evaluation. Etchants were dependent on composition and alloying element. Vickers hardness measurements were used for a quick and qualitative evaluation of the strength dependence on alloy composition.

4. RESULTS

Baseline experiments using matrices of 316L SS and elemental iron were made as references for typical sample soundness under specific operating conditions and to determine the effect of using different types of iron powder. Both iron and manganese were first added to the 316L SS to determine the effects of powder type and composition on the metallurgical integrity of the fabricated alloys. Manganese and nickel were added to iron for studies of the binary systems.

4.1. SET 1: Reference Matrices: Atomized 316 SS, Sponge Iron

A considerable amount of work has been done with 316 S atomized powder, both at Sandia and on practically every LENS machine made [1-23]. This set of experiments was run to demonstrate that the machine was in good working order. Because neither gas atomized manganese or iron powder was readily available at the project's start, the initial experiments evaluated the effect of sponge iron additions to gas atomized 316 SS. This was done to determine whether the processing conditions developed for 316 would also be appropriate for the elemental iron. The 316 SS alloy was modified to evaluate the effects of increased iron on material and mechanical properties. These experiments were done using both open loop control (melt pool sensor off), and closed loop feed back control of the laser power to maintain a constant melt pool size. The light intensity at a particular laser power setting changed the amount of light given off by the melt pool and led to changes to the optics for the closed loop sensor. Open loop processing was used and laser power adjusted to set the light intensity (and therefore the temperature during deposition). Only samples made with 316 were essentially pore free, while those with iron contained considerable porosity as shown in Figure 4.

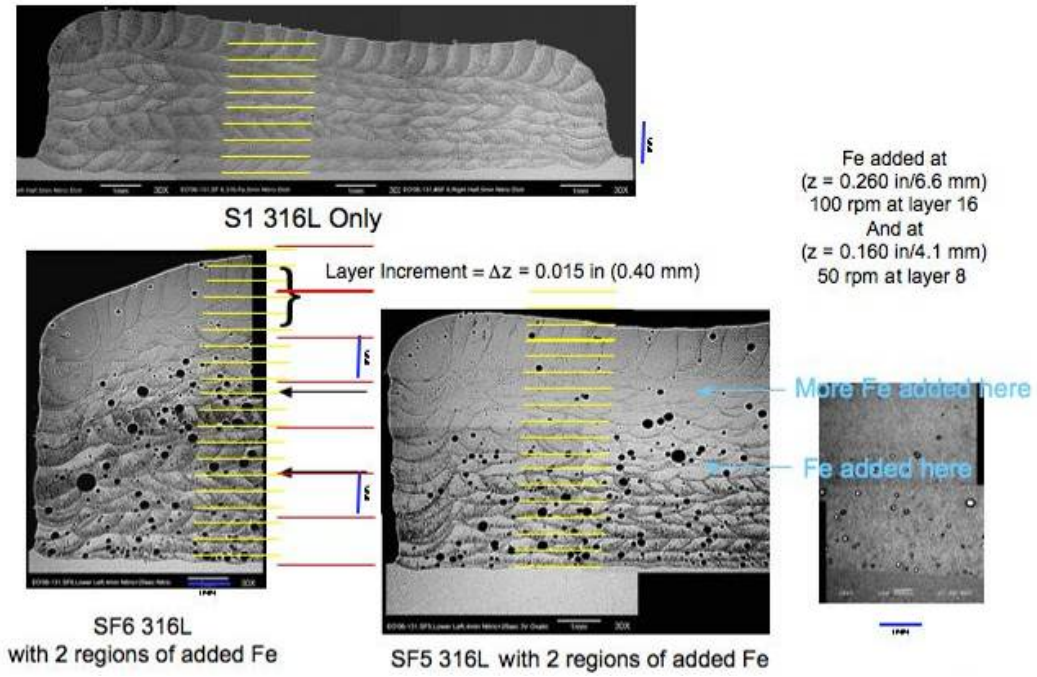

Figure 4. Cross-Sections of Three Samples with 316L Only (top), and Fe Added at Two Values in Open Loop (left) and Closed Loop (right) Control Modes.

For the first experiments two distinct changes in composition were made at 4.1 mm and 6.6 mm, by increasing the feed rate for the iron powder and decreasing the feed rate on the 316 SS. Iron content was measured at 70, 72 and 75% by EDS, corresponding to iron powder feed rates of 0, 50 and 100 rpm respectively. Each 50 rpm corresponded to about 2.5 % iron. At the higher iron powder feed rate, and further away from the substrate, the porosity decreased significantly. With the increases in the amount of iron, the Vicker's hardness increased from an Hv of 200 to Hv of 300 (100g load). The pure iron samples did not behave as well as the 316 SS, and noticeable flaring of the melt pool was observed, driving the melt pool sensor to saturation. This resulted in a very porous sample with thinner layers deposited per scan than the z-height increment from one layer to another. Consequently, the samples stopped building before the final scan height was reached.

4.2. SET 2 (A) Baseline 316L SS "Alloys": Fe vs. Mn

A second set of iron added to 316L SS experiments were carried out with somewhat different processing conditions to reduce the porosity. At the same time, a set of manganese added to 316L experiments were carried out, again to determine how the composition affects the size and intensity of the light emitted from the melt pool, as well as to determine if the porosity could be reduced or eliminated. There was a very distinct change in the intensity with increased manganese (see sections 3.2.2 and 3.2.3). It was not possible to use the feedback control loop to maintain constant melt pool size, so both experiments were done using open loop conditions. For these experiments, the composition was changed at 0.125, 0.250, and 0.375 inches (3, 6, and 9 mm). Nominal powder feed rate was 400 rpm for the 316, and the alloying element feed rate was 0, 50, 100, or 150 rpm, with the 316 SS powder feed rate 400, 350, 300, and 250 rpm. See Table 3 for conversions of rpm to expected part compositions. Samples were intended to be 0.5 inches (12.5 mm) high. Figure 5 shows the iron content increased incrementally at the nominal 69 %, to 72, 75, and 79%, and the manganese from nominal 1.5 % to 13, 20, and 31%. A plot of the other element variations is shown on Figure 6. The larger amount of porosity near the base of the samples in Figure 5 indicates that either the process parameters were better suited for the increased alloying element content found near the top of the sample, or that the focus height for depositing was not optimized and the part "grew" into the correct focus as it built.

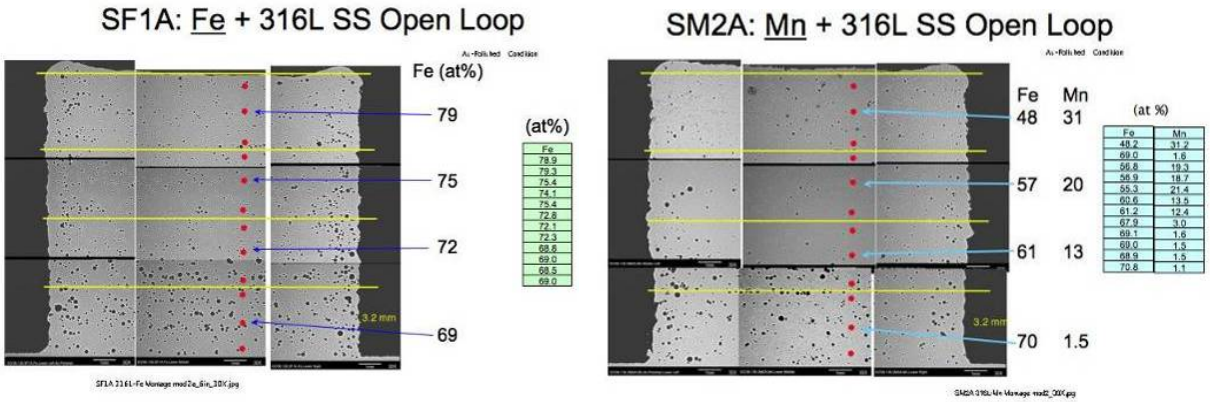

Figure 5. The As-Polished Samples Indicate that the Uniformity in Cross Section is Better in Open Loop than Closed Loop Control, but Porosity Is Still above Acceptable Levels in Both.

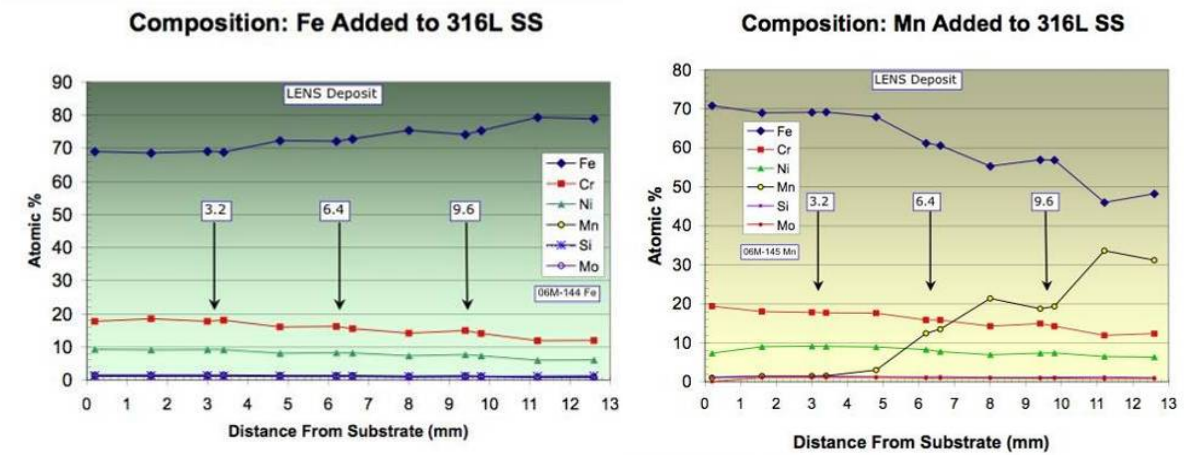

Figure 6. Composition Profiles for Iron Added to 316L SS (left), and Manganese Added to 316L SS (right).

The corresponding hardness showed a decrease for manganese additions, and an increase for iron additions (See Figure 7). Iron had the stronger effect, raising the Vicker's hardness (100g load) from 225 to over 350 for an iron increase of about 6%. Addition of manganese slightly lowered the hardness for a content of about 20 %Mn.

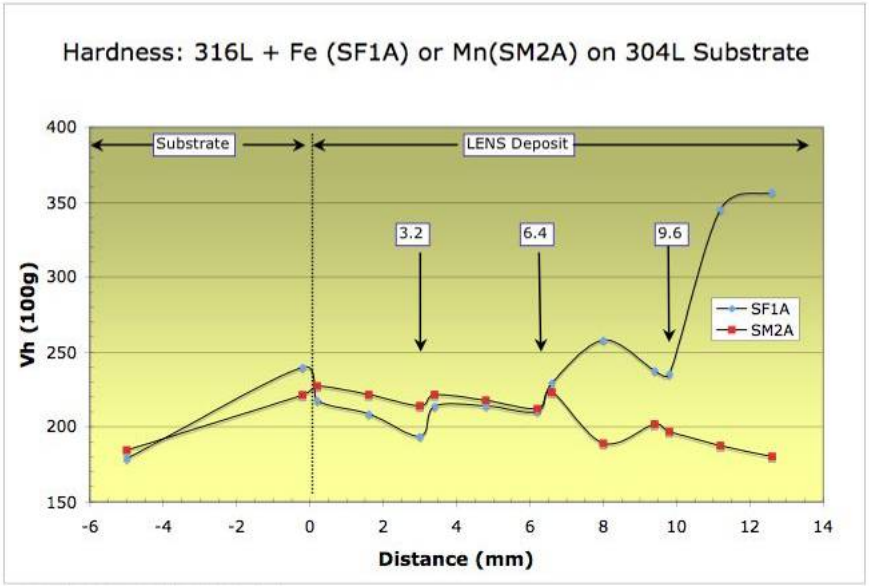

Figure 7. Hardness Profiles for Iron (SF1A) and Manganese (SM2a) Added to 316L SS.

Of interest was the lack of complete melting of the stainless steel particles, as seen in the wavelength dispersive X-RAY (WDS) mapping of the 30%Mn sample region (See Figure 8). While the stainless steel was fully melted in alloying with Mn compositions less than 30%, once this composition was reached, the stainless no longer fully melted. This was unexpected by the team. When unmelted particles were first noticed in micrographs, it was expected that these would be Mn caused by reaching some saturation point, but evaluation showed this assumption to be incorrect.

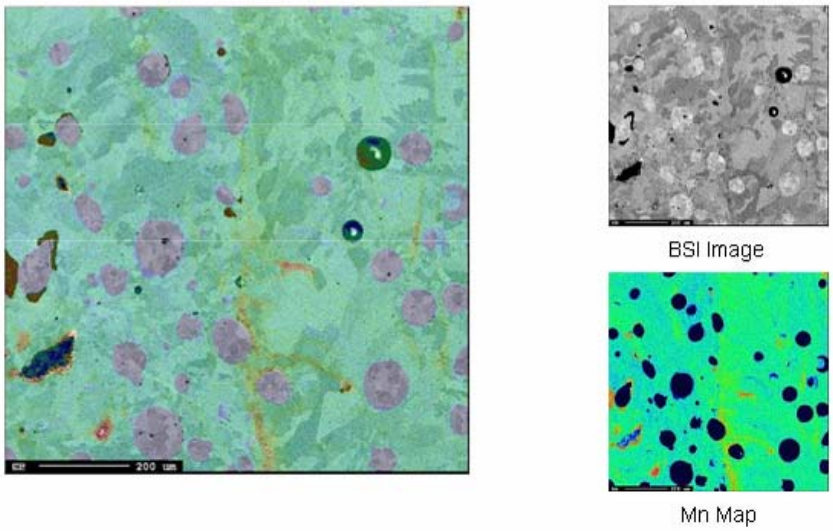

Figure 8. Composition Map Showing Overlay of BSE Image and Mn Distribution (light green hue), Indicating Incomplete Melting of the Stainless Steel Particles.

4.3. SET 3 (B) Fe-10%Mn; Fe-14%Mn Alloys: Atomized Iron:

In this case, iron was used as the base element instead of the stainless steel, and a different iron powder was used. This experiment used Ancorsteel 1000B water atomized iron with particle size -100 +325mesh (44 to 150µm). For these experiments, deposition was done at 20 ipm, 25 amps power, 405 rpm Fe/45 rpm Mn, and 20 ipm, 25 amps power, 387 rpm Fe/63 rpm Mn, for the 10 and 14 pct manganese samples. Two samples of just iron were deposited, but did not build well. Two samples with Mn (one at 10%, and the other at 14 %) were also built, and they did build better. It was noted that the atomized iron powder produced better deposits than the sponge iron, where the porosity was reduced but not completely eliminated. Figure 9 shows the porosity increasing with sample height and evidenced by lack of interlayer metallurgical bonding. Recorded Vicker's hardnesses were 109 and 116 for the pure iron, while values of 281, and 285 were measured for the 10 % and 14 % Mn alloys respectively.

4.4. SET 4 (D) Atomized Iron Only; Closed Loop Control:

In an attempt to improve deposition conditions, this set of experiments was run with closed loop control using a threshold intensity setting of 200. Two 0.5" (12.7mm) cubes were built under slightly different processing conditions, and a "horizontal tower" was built for tensile property evaluation. The first sample did not build very well. Travel speed was decreased and powder flow rate increased for sample F3D. The laser power fluctuated from 745 to 860 watts. For the horizontal "tower", the focal point of the laser was embedded at 0.150" (3.8mm) instead of 0.175" (4.8mm). Laser power in this case fluctuated from 575 to 800W, considerably lower than for the square cube samples.

Quantitative image analysis was used to determine the amounts of porosity for these samples. Because of the unacceptable porosity, no mechanical properties were measured. Figure 10 shows these samples which have a relative porosity of 1%.

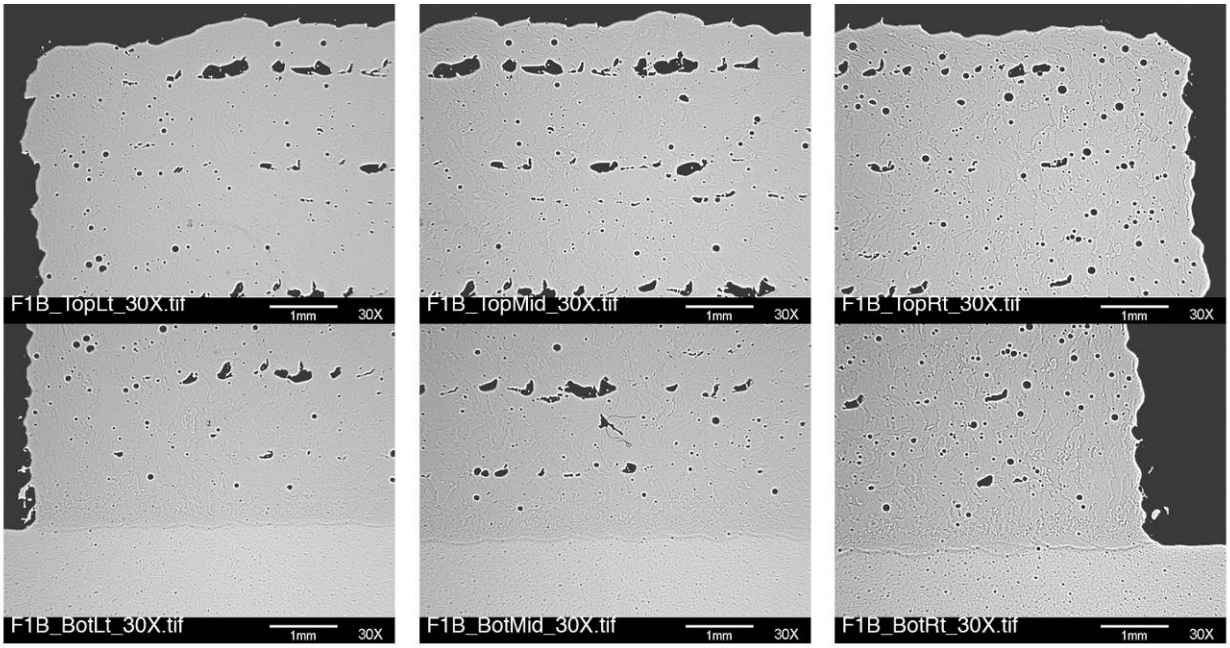

Figure 9. As-Polished Cross Section of Sample F1-B, Showing Porosity and Poor Inter-Layer Bonding.

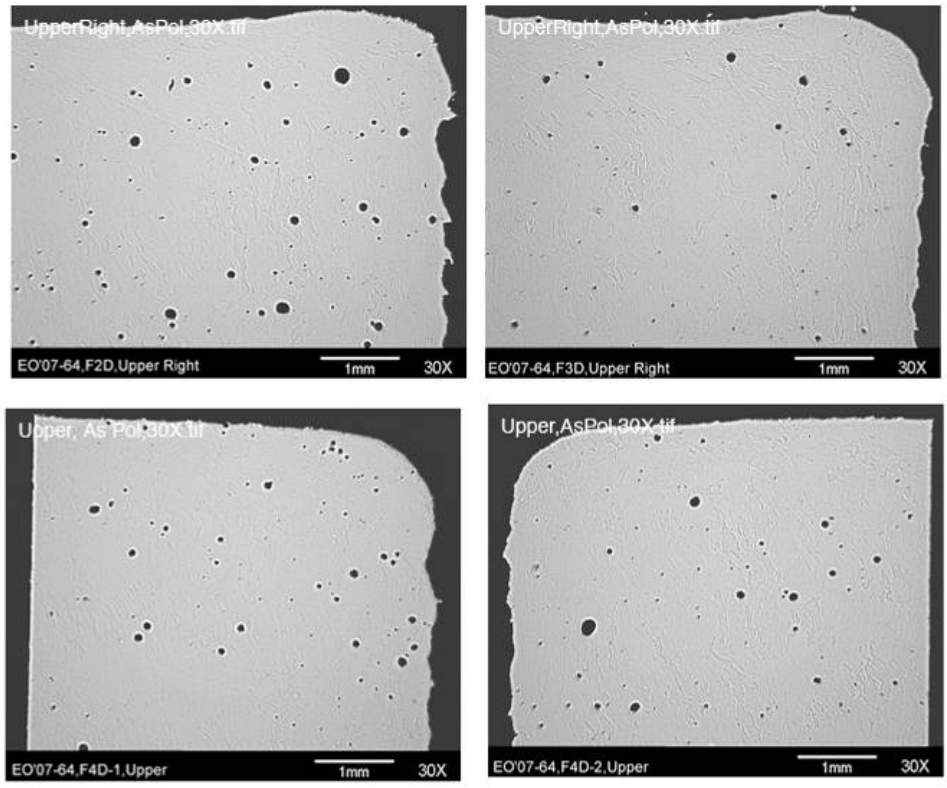

Figure 10. Polished Cross Sections of the Pure Iron Cubes (F2D, F3D) and the Horizontal Tensile Bar (F4D-1, F4D-2), Showing 1% Porosity.

4.5. SET 5 (E) Four Fe-Mn Alloy Tensile Bars: Closed Loop Control

Despite the disappointment of unacceptable porosity, it was decided to attempt fabrication of some Fe-Mn alloys in horizontal tower configuration for tensile property and microstructure analysis. Three samples were fabricated, two (Case I) with 0, 5, 10, and 20% Mn, and one (Case II) with 25, 50, and 75 % Mn. as shown schematically in Figure 11. The horizontal configuration is ideal for making flat tensile bars for mechanical property evaluations, and by making them longer than needed for the tensile bar, also provides coupons for metallography. In this case each sample was made with four different compositions with each composition being four layers thick. The layers are nominally 0.020" (0.5mm) thick, so each composition is roughly 0.080" (2.0mm) thick. The part and measured compositional Mn% are shown in Figure 12.

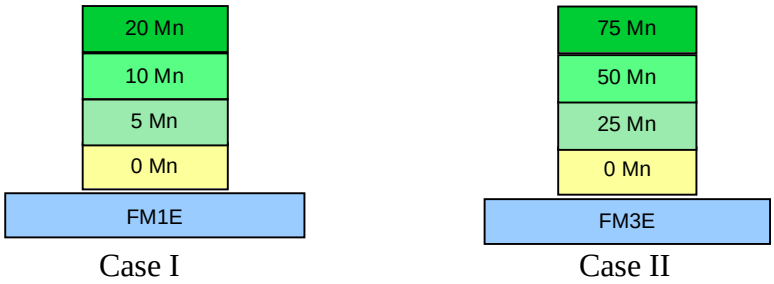

Figure 11. Schematic Cross Sections of FeMn Showing Target Compositions Under Closed Loop Control.

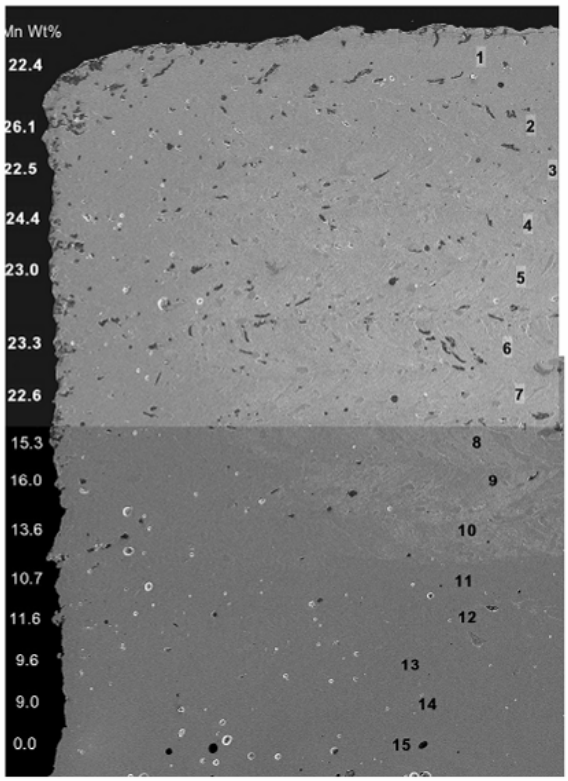

Figure 12. Cross Section of FeMn Sample FM1E with Location and Measured Composition Mapped on Surface.

Deposition conditions for sample FM1E are the same as FM2E, with PID on, intensity set at 220, delta z and hatch at 0.020" (0.5mm), 650/620/265, and 18ipm (7.62mm/s) feedrate. The powder feeder setting was 525RPM (26.5g/min) and laser power observed to vary between 35 and 40 amps. Immediately after starting feeder #2, the weld pool image changed drastically and power dropped down to 420 W (26amps). Powder feeder settings had the following ratios (%Fe %Mn) (100/0), (95/5), (90/10), (85/15) at the build heights of 0.0, 0.080, 0.160, and 0.240 inches (0.0, 2.0, 4.0, and 6.0mm) respectively.

4.6. SET 6 (F) Four Fe-Mn Alloy Tensile Bars, Closed Loop Control; Duplicates

For this set of experiments, intended to duplicate SET 5 E, two-inch long bars were deposited with a 3/8-by-3/8 cross-section for tensile bar testing. Again, four compositions, each about 0.080 inches thick were deposited one on top of another. For one bar (FM25-1F), the compositional ratios (Fe/Mn) were nominally 100%Fe, Fe-10%Mn, Fe-20%Mn, and Fe-25%Mn. For the other (FMX-2F), the compositions were nominally 100%Fe, Fe-25%Mn, Fe-50%Mn, and Fe-75% Mn. The experiments were done with the closed loop controller on and set to a threshold intensity of 220. The microstructure showed that these samples contained considerable porosity, as shown in the microstructures in Figure 13. The hardness for these samples was measured and is presented in Figure 14 showing an initial increase in hardness to 10%Mn with no further increase up to 75%Mn.

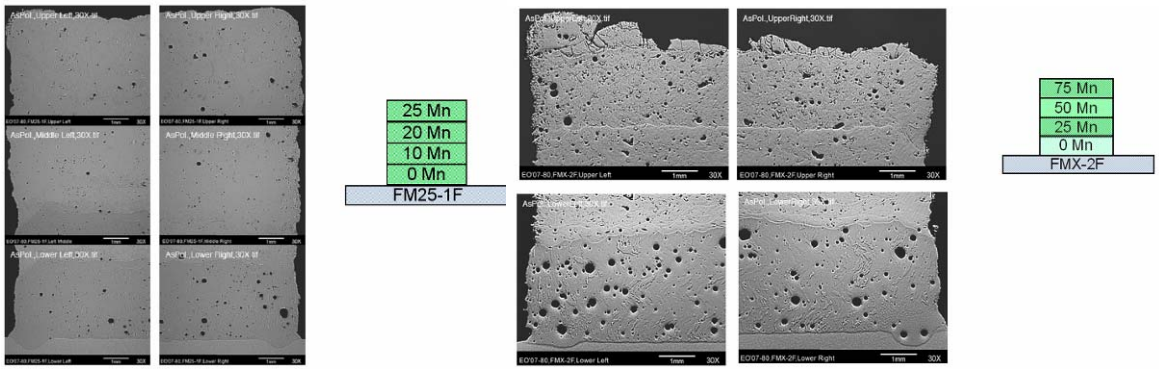

Figure 13. As-Polished and Schematic Cross Sections of the FeMn Sample FM25-1F(left) and FMX-2F (right) Showing Target Compositions, Interface Regions, and Porosity.

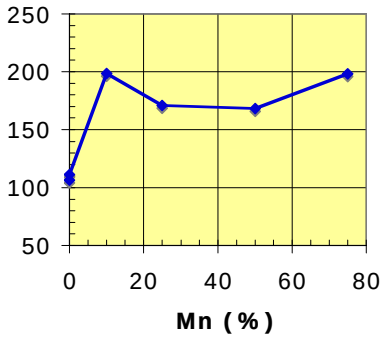

Figure 14. Plot of Hardness vs. Mn Content Indicating an Initial Increase with 10 % Mn Levelling to 75% Mn.

4.7. SET 7 (G) Fe-20Mn, Fe-10Mn: Effect of Threshold Setting

In an attempt to decrease the porosity in the alloyed material, an experiment was conducted in which the threshold setting (and thus the laser power) was varied through builds of two different compositions. The threshold setting is a unitless number representing the perceived intensity of pixels within the melt pool. The closed loop controller uses the threshold value to create an enclosed region of pixels with intensity greater than the threshold value. The controller then attempts to adjust the laser power to maintain this enclosed region at a specified area. The threshold settings for Fe-10%Mn were 200, 250, 300, and 350. The threshold settings for Fe-20%Mn were 355, 450, 480, and 480.

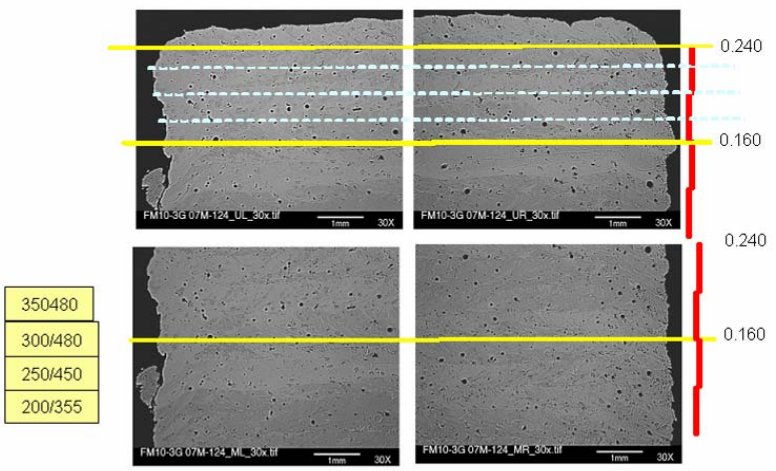

Figure 15. Schematic Cross Section of Fe-10% Mn and Fe-20% Mn Samples and Polished Cross Section of Fe-10% Mn Showing Porosity, Layer Interfaces (Dotted Lines) and Threshold Setting Changes.

As can be seen in Figure 16, the laser power increases with increasing threshold setting and is higher for 10% Mn alloy than the 20% Mn alloy. This indicates that it takes less power to deposit the higher manganese alloy for a given melt pool size. Lower power resulted in reduced porosity, though porosity was not eliminated for any reasonable settings under which parts could be produced. This does suggest that processing parameters affect porosity.

4.8. SET 8 (H) Fe-5, 10, 20% Ni: Filter Density Effect: 200 vs. 180%

In addition to the threshold setting, another process variable for the closed loop control system is the camera filter. This filter is a neutral density filter that reduces the intensity of the melt pool light incident on the camera. The filter is necessary to prevent saturation of the camera, but it is possible to overdamp the light signal such that the camera is not able to discern the intensity differences in the melt pool sufficiently well. The filter percentage is related to the optical density (OD), so a 100% filter increases the system absorbance by one OD. Thus, it is possible to have filters with percentages in excess of 100%. A higher filter number also allows the aperture of the camera to be changed which can have many other effects on depth of field, distortion, etc. For the filter test, two filter settings of 180% and 200% were used for depositing FeNi at 4 different compositional settings. The samples are shown in Figure 17 and Figure 18. The materials showed no effect of these two filter settings on the alloy composition or on the size and density of the porosity. In addition, hardness values were inconclusive, as shown in Figure

19, but roughly show the hardness to increase with nickel content reaching a 10 % Ni and then reducing until 20 % nickel is reached.

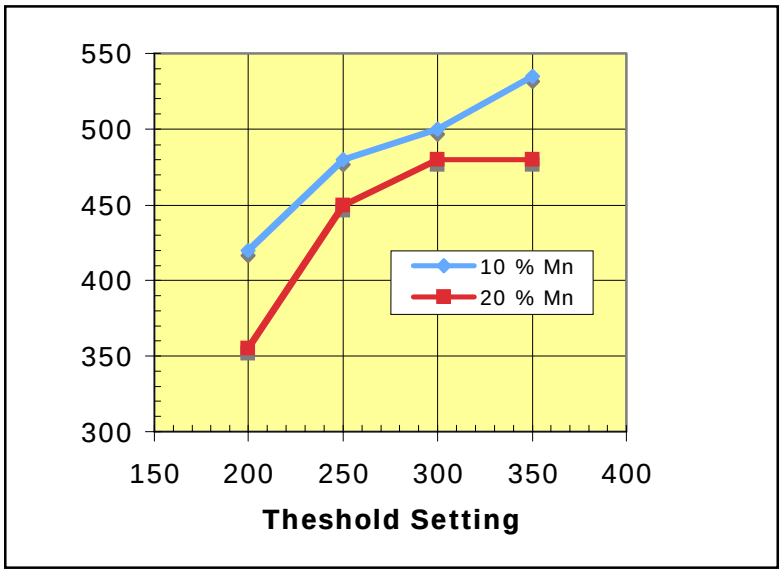

Figure 16. Plot of Laser Power (Watts) vs. Threshold Settings for Fe-10% Mn and Fe-20% Mn Showing that Increased Mn Content Reduces the Power Required to Maintain a Specific Melt Pool Size.

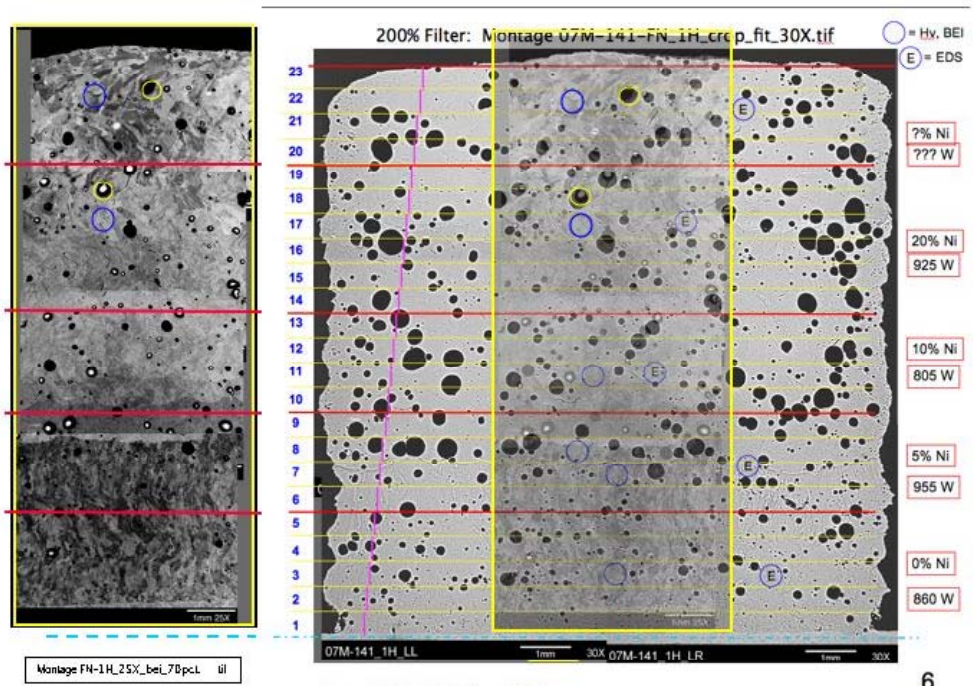

Figure 17. Cross Section of Sample FN1H for Filter Setting of 200% and Threshold Intensity of 200, Showing Variation of Porosity with Composition.

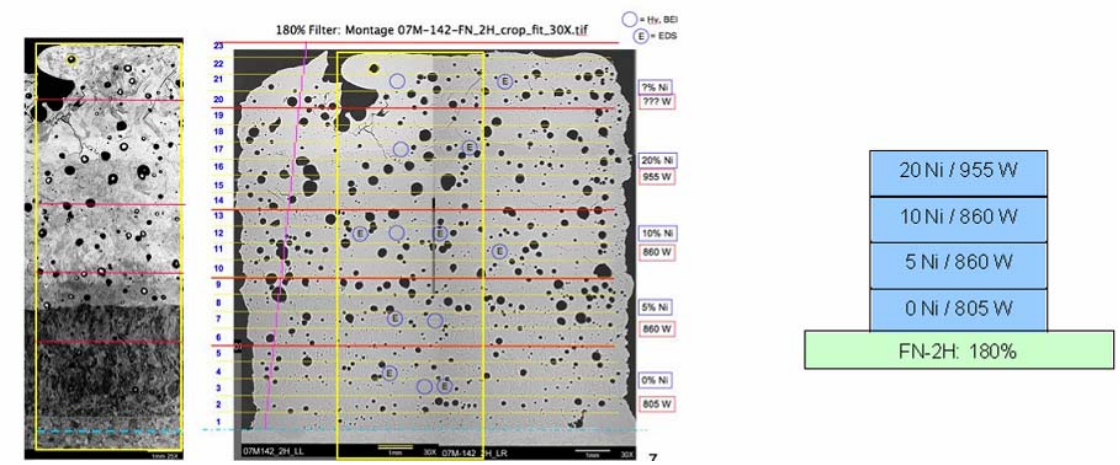

Figure 18. Cross Section of Sample FN-2H for Filter Setting of 180% and Threshold Intensity of 200, Showing Variation of Porosity with Composition.

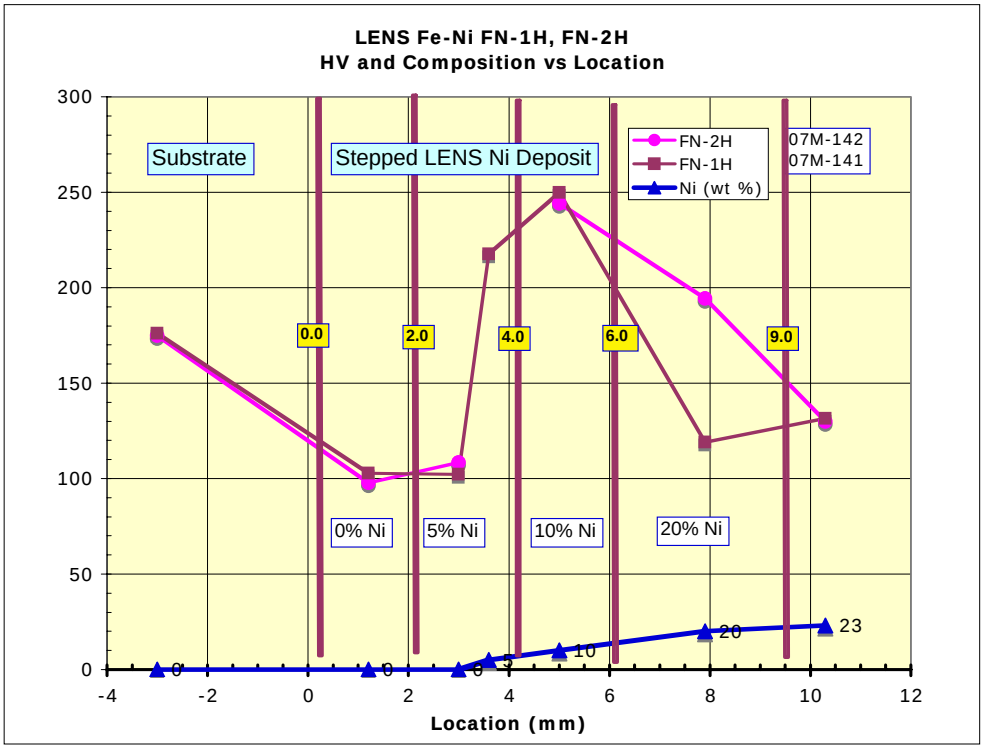

Figure 19. Hardness Profile with Location and Nominal Compositions for the FeNi Binary System.

4.9. SET 9 (J) Fe-20% Ni: Effect of Laser Power; 355, 480, 650, 955W

Because of the lack of the ability to eliminate porosity using the closed loop control parameters, the system was run in open loop mode where a specific laser power is set and maintained throughout a build. For this set of experiments, the Ni content was held at 20% and the laser power was changed every 4 layers. Figure 20 shows the difference in structure achieved with the lowest (355W) and highest (955W) power settings. The higher power increases the size of the pores, but also eliminates the inadequate inter-layer bonds seen at the lower power. In both cases, there seemed to be very little substrate melting.

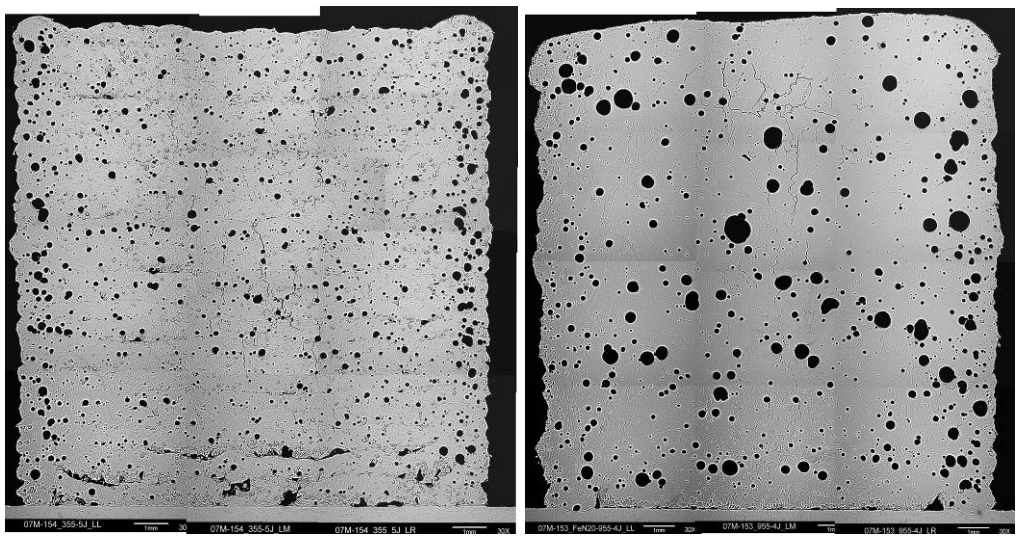

Figure 20. Cross Section of Fe-20%Ni Samples Deposited with Laser Power of 355W (left) and 955W (right) Showing an Increase in Pore Size and Inter-Layer Bonding with Increased Power.

4.10. SET 10 (K) Fe-20% Mn: Effect of Laser Power; 245, 355, 480, 650W

The tests of Set 9 were repeated with Mn in alloy composition of Fe-20%Mn. The laser power levels chosen for this experiment were 245, 355, 480, and 650W which are all in the typical operating range. The 245W and 650W samples are shown in Figure 21 and, similarly to the Ni experiments, the samples showed a lack of bonding at lower power and an increase in the size of the porosity at higher power. However, the overall amount of porosity at the higher power level appears to be significantly reduced.

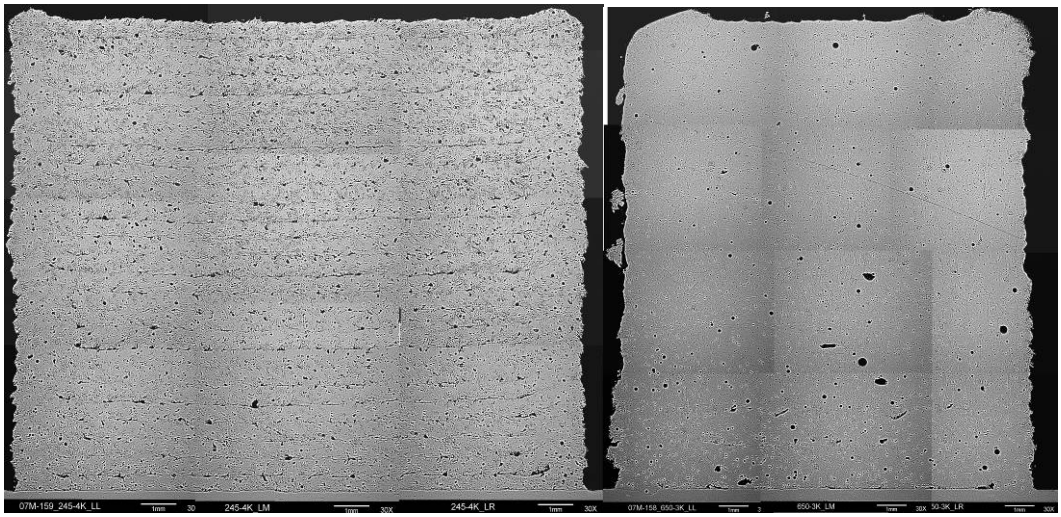

Figure 21. Cross Section of Fe-20%Mn Samples Deposited with Laser Power of 245W (left) and 650W (right) Showing an Increase in Pore Size and Inter-Layer Bonding with Increased Power.

5. DISCUSSION

5.1. Reference Experiments

Initial experiments started with gas atomized 316 SS, as a baseline to confirm that the LENS machine was in fact operating as it has for a "standard alloy", one that has undergone extensive studies for development of the LENS technology. Results indicated full density, but the top of the deposits were not flat. Addition of the sponge iron introduced considerable porosity, not seen before in 316SS, and attempts to rectify the porosity by changing process parameters were unsuccessful.

The water atomized iron powder was then tried as an alternative, and it produced considerably better results. Graded compositions were readily achieved and the alloying additions resulted in hardness changes in the 316. Iron produced a hardening effect, raising the Vicker's hardness from 225 to over 350, and manganese produced a softening effect, resulting in a reduction in hardness from 225 to about 180.

Experiments were done in both open loop and closed loop control to set the solidification conditions and to determine if one could also control microstructure features with process control. There were mixed results. This was due mainly to the difference in emissivity of the alloying elements, causing the sensor to saturate and cause the laser power to change dramatically from the baseline 316SS processing conditions. Considerable distortion of the melt pool sensor images led to changes in experimentation to overcome the increased image intensity. The sensor was modified to allow interchange of light filter density to keep image intensity within range of camera capability. This helped but did not result in eliminating porosity nor did it result in squared off edges to the deposits. Experimental results showed that iron added to 316 provided additional strength, while manganese had a softening effect.

5.2. Iron-Manganese and Iron-Nickel Systems

For these binary systems, experiments were carried out in open loop to prevent the laser from taking radical power changes associated with the excess light intensities. Here the modification was made to the apparatus to introduce fixed density filters to compensate for the differences in brightness during alloying. Hence there is a need to further develop the melt pool sensor to adjust for differences in intensity, which was beyond the scope of this project.

Despite all the attempts to maintain stable processing conditions and achieve porosity free deposits, the alloys were plagued with excessive porosity, and alternate experiments were undertaken to reduce and/or eliminate the porosity before extensive metallographic and mechanical property studies were initiated. Experiments were conducted to show the differences in laser power and composition for a series of samples of Fe-Mn alloys. The results are documented above. Additional experiments showed the ability to make layered samples long enough to fabricate flat dog-bone tensile specimens for a variety of compositions, but due to the porosity, the samples were never machined. Assessments of the microstructure were limited to a determination of the porosity and in some cases to the actual composition via EDS or microprobe analysis.

Nickel on the other hand was an atomized powder and the porosity was expected to be lower than the manganese. While this was the case, the samples were still plagued by porosity. However, the hardness for the Fe-Ni alloys was measured and a hardening peak was observed at 10 % nickel. Experiments showed the size and distribution of the pores to vary with laser power, and composition, but never enough to satisfactorily eliminate porosity. The cause of the porosity remains a major mystery at this point. For the FeNi alloys, higher power produced better inter-layer metallurgical bonding, but also larger pores. For the FeMn alloys, the porosity was much finer at both low and high laser power. Again the inter-layer bonding was bad at low power, but better at high power. The average pore sizes of the FeMn alloys produced with the higher power were much finer and occupied a smaller volume fraction than at low power.

5.3. Appropriateness of the Technique

The results neither proved nor disproved the postulation that LENS could be used for rapid alloying studies and for the creation of materials with unique properties. Unfortunately, the porosity problems exhausted the time and financial resources available for this study. The team's evaluation of the process produced the speculation that other metal powders might have superior performance characteristics than those tried here. In any case, the porosity must be eliminated for the technique to be utilized in time-critical alloying studies.

Curiously, during the course of this project, it was noted that other LENS researchers at University of California, Davis, and at The Ohio State University had also had problems with increased porosity, even when working with standard LENS materials such as 316L and Ph13-8Mo. While this could be a coincidence of timing or of researchers pushing the boundaries of the processing envelope, it could also point to a process change in the metal powder industry. Indeed, for this project, the acquisition of metal powder caused significant delays as the standard powder suppliers seemed to experience process failures and a change in priorities away from this group of researchers. It is hoped that future communication among researchers at LENS Users' Groups and at relevant conferences will help to identify whether this phenomenon is real or imagined. Until proven otherwise, though, it would be prudent for additional studies to be started to clearly identify the source of the porosity in both traditional and highly experimental alloys.

6. CONCLUSIONS

The project team successfully showed the methods needed to rapidly prototype material systems for creating new alloys. This consisted of using the LENS® laser metal deposition technology with multiple powder feeders to make small test coupons for evaluating microstructure and composition, as well as to identify new phases as a function of composition and processing conditions. This technique allows for many alloy samples to be made using a minimal quantity of material and time. While the ability to make many alloy samples was demonstrated, results were tempered by a level of porosity not experienced in previous work using pre-alloyed, gas atomized, metal powders. The focus of the work shifted to eliminating the porosity using a variety of processing parameter combinations instead of making different alloy compositions and to dealing with differences in emissivity associated with the alloying elements and their impact on control of melt conditions. Laser power, travel speed, powder type, powder feed rate, sensor filter setting/type, melt pool size, open and closed loop control, deposit track overlap, and layer height increment were tested in attempts to eliminate porosity. While variations in the material's microstructures were observed, porosity continued to remain as an obstacle to realizing metallurgically sound alloys for mechanical property determination.

Programmatically, the challenge and thus the time and funding required to achieve success were underestimated. This underestimation, compounded by an apparent lack of elemental powder availability in the type, quality and size needed for LENS depositing greatly reduced the impact of this research. The team discovered that sources of high quality powder in small to medium quantities are difficult to obtain on short notice, because either vendors do not want to be making special heats of powder or because there is a backlog for such orders.

So, while a disproportionate percentage of the metallographic analysis was utilized to address the porosity challenge, some interest was sparked for gas transfer systems and fusion energy first wall diffusion barrier material systems for graded materials. As a next step, the team intends to pursue development projects with both these communities. Additional customer interest is in making and repairing W87 fuze supports (which are otherwise not available due to the unavailability of older processing technologies) both with and without coatings for reliability testing. In addition, studies to optimize processing parameters and powder characteristics to complete the achievement of full density are needed.

The key accomplishments of the project were the exploration of alloy modifications of 316L stainless steel, and iron alloys with Mn and Ni added as individual elements for Sandia applications. The team evaluated microstructure and hardness of the base metals as a function of Mn and Ni, and of 316 SS as function of Fe and Mn content. In addition, the team investigated the effects of laser power and camera filter on the density of alloys, and demonstrated the ability to achieve gradients in composition or layers of specific compositions in single small test samples. A peak in the hardness of Fe-Ni alloys of about 10 % Ni was observed.

7. REFERENCES

[1] C. Atwood, M. Griffith, L. Harwell, E. Schlinger, M. Ensz, J. Smugeresky, J. A. Romero, D. Greene, and D. Reckaway, "Laser Engineered Net Shaping (LENS™): A Tool for Direct Fabrication of Metal Parts," in *ICALEO '98; The International Congress on Applications of Lasers and Electro-Optics*, Orlando, FL, 1998, p. Paper # 801.

[2] C. L. Atwood, M. L. Griffith, L. D. Harwell, D. L. Greene, D. E. Reckaway, M. T. Ensz, D. M. Keicher, M. E. Schlienger, J. A. Romero, M. S. Oliver, F. P. Jeantette, and J. E. Smugeresky, "Laser Spray Fabrication for Net-Shape Rapid Product Realization LDRD," Sandia National Laboratories, Albuquerque, NM SAND99-0739, April, 1999 1999.

[3] M. L. Griffith, M. T. Ensz, J. D. Puskar, C. V. Robino, and J. A. Brooks, "Understanding the Microstructure and Properties of Components Fabricated by Laser Engineered Net Shaping (LENS)," *Performer: Sandia National Laboratories*, vol. 18, pp. SAND2000-1000C, 2000.

[4] M. L. Griffith, L. D. Harwell, D. L. Greene, J. A. Romero, T. Bucheit, T. Crenshaw, and V. Tikare, "Materials and Properties of Components Formed Using the 3D Wire Process," in *PRICM3 Advanced Materials Processing*, Honolulu, Hawaii, 1998, p. 3074.

[5] M. L. Griffith, W. H. Hofmeister, G. A. Knorowsky, D. O. MacCallum, M. E. Schlienger, and J. E. Smugeresky, "Direct Laser Additive Fabrication System with Image Feedback Control," 2002.

[6] M. L. Griffith, D. M. Keicher, C. L. Atwood, J. A. Romero, J. E. Smugeresky, L. D. Harwell, and D. L. Greene, "Free Form Fabrication Of Metallic Components Using Laser Engineered Net Shaping (LENS™)," in *Solid Freeform Fabrication Symposium*, Austin, TX, 1996.

[7] M. L. Griffith, M. E. Schlienger, and L. D. Harwell, "Thermal behavior in the LENS process," *Performer: USDOE Office of Financial Management and Controller, Washington, DC*, vol. 31, pp. CONF-980826, 1998.

[8] M. L. Griffith, M. E. Schlienger, L. D. Harwell, M. S. Oliver, M. D. Baldwin, M. T. Ensz, M. Essien, J. Brooks, C. V. Robino, and e. J. E. Smugeresky, "Understanding thermal behavior in the LENS process," *Materials and Design (UK)*, vol. 20, pp. 107-113, June 1999.

[9] M. L. Griffith, M. E. Schlienger, L. D. Harwell, M. S. Oliver, M. D. Baldwin, M. T. Ensz, M. Essien, J. Brooks, C. V. Robino, J. E. Smugeresky, W. H. Hofmeister, M. J. Wert, and D. V. Nelson, "Understanding Thermal Behavior in the LENS® Process," *Materials and Design*, vol. 20, pp. 107-113, 1999.

[10] W. Hofmeister, M. Griffith, M. Ensz, and J. E. Smugeresky, "Solidification in Direct Metal Deposition by LENS Processing," *JOM*, vol. 53, pp. 30-34, 2001.

[11] D. M. Keicher, J. L. Jellison, L. P. Schanwald, J. A. Romero, and D. H. Abbott, "Towards a Reliable Laser Spray Powder Deposition System Through Process Characterization," in *SAMPE 1995*, Albuquerque, NM, 1995, pp. 1009 -1018.

[12] D. M. Keicher, J. A. Romero, C. L. Atwood, J. E. Smugeresky, M. L. Griffith, F. P. Jeantette, L. D. Harwell, and D. L. Greene, "Free Form Fabrication using the Laser Engineered Net Shaping (LENS™) Process," in *PM2TEC '96*, Washington, DC, 1996.

[13] D. M. Keicher, J. A. Romero, F. P. Jeantette, and e. al, "Laser based engineered net shaping device," USA: Sandia National Laboratories/DOE, 1996.

[14] D. M. Keicher and J. E. Smugeresky, "The Laser Forming of Metallic Components Using Particulate Materials," *JOM*, pp. 51-54, 1997.

[15] D. M. Keicher, J. E. Smugeresky, J. A. Romero, C. L. Atwood, M. L. Griffith, F. P. Jeantette, L. D. Harwell, and D. L. Greene, "Laser Engineered Net Shaping (LENS™) for Additive Component Processing," in *SME Conference*, Dearborn, MI, 1996.

[16] D. M. Kiecher and J. E. Smugeresky, "Review of Laser Forming Using Particulate Materials," Sandia National LAboratoires, LIvermore, CA SAND97-XXXX, July 1997.

[17] J. E. Smugeresky, D. M. Keicher, J. A. Romero, and e. al., "LENS™ Processed Incoloy 625," *Submitted to MS&E*, 1997.

[18] J. E. Smugeresky, D. M. Keicher, J. A. Romero, M. L. Griffith, and L. D. Harwell, "Laser Engineered Net Shaping (LENS™) Process: Optimization of Surface Finish and Microstructural Properties," in *PM2TEC '97*, Chicago, IL, 1997, pp. 21-33, 21-42.

[19] J. E. Smugeresky, M. E. Schlienger, M. Oliver, and J. A. Romero, "Effect of LENS™ Processing on Mechaniccal Properties of Ti 6Al-4V," 1998.

[20] D.D. Gill, J.E. Smugeresky, C.V. Robino, M.F. Harris, and M.L. Griffith, "On the Interface Between LENS® Deposited Stainless Steel 304L Repair Geometry and Cast of Machined Components", December 2008, SAND2004-4035, Sandia National Laboratories, Albuquerque, NM

[21] D. Gill, J. Smugeresky, C. VanCamp, T. Adams, and J. Oberhaus, "LENS Repair and Modification of Metal NW Components: Materials and Applications Guide", November 2006, SAND2006-6430, Sandia National Laboratories, Albuquerque, NM

[22] D.D. Gill, J.E. Smugeresky, C.J. Atwood, M.D. Jew, and S. Scheffel, "Process Qualification and Testing of LENS® Deposited AY1E0125 D-Bottle Brackets", November 2006, SAND2006-6431, Sandia National Laboratories, Albuquerque, NM

[23] D.D. Gill, J.E. Smugeresky, C.J. Atwood, "Laser Engineered Net Shaping™ (LENS®) for the Repair and Modification of NWC Metal Components", November 2006, SAND2006-6551, Sandia National Laboratories, Albuquerque, NM

DISTRIBUTION

Sandia National Laboratories – Internal Mailings

1	MS0123	Donna Chavez, LDRD	1011
4	MS1245	David Gill	2455
1	MS1245	Clinton J Atwood	2455
5	MS9402	John E. Smugeresky	8758
1	MS9402	Rion Causey	8758
1	MS0899	Technical Library	9536 (electronic copy)
1	MS0123	Donna Chavez, LDRD	1011 (electronic copy)


Sandia National Laboratories